Review

Dielectric Barrier Discharge Plasma-Assisted Catalytic CO$_2$ Hydrogenation: Synergy of Catalyst and Plasma

Xingyuan Gao [1,2,3], Jinglong Liang [1], Liqing Wu [1], Lixia Wu [1] and Sibudjing Kawi [3,*]

1 Department of Chemistry and Material Science, Guangdong University of Education, Guangzhou 510303, China; gaoxingyuan@gdei.edu.cn (X.G.); liangjinglong@gdei.edu.cn (J.L.); wliqing@gdei.edu.cn (L.W.); wlixia@gdei.edu.cn (L.W.)
2 Engineering Technology Development Center of Advanced Materials & Energy Saving and Emission Reduction in Guangdong Colleges and Universities, Guangzhou 510303, China
3 Department of Chemical and Biomolecular Engineering, National University of Singapore, Singapore 117585, Singapore
* Correspondence: chekawis@nus.edu.sg; Tel.: +65-65166312

Abstract: CO$_2$ hydrogenation is an effective way to convert CO$_2$ to value-added chemicals (e.g., CH$_4$ and CH$_3$OH). As a thermal catalytic process, it suffers from dissatisfactory catalytic performances (low conversion/selectivity and poor stability) and high energy input. By utilizing the dielectric barrier discharge (DBD) technology, the catalyst and plasma could generate a synergy, activating the whole process in a mild condition, and enhancing the conversion efficiency of CO$_2$ and selectivity of targeted product. In this review, a comprehensive summary of the applications of DBD plasma in catalytic CO$_2$ hydrogenation is provided in detail. Moreover, the state-of-the-art design of the reactor and optimization of reaction parameters are discussed. Furthermore, several mechanisms based on simulations and experiments are provided. In the end, the existing challenges of this hybrid system and corresponding solutions are proposed.

Keywords: CO$_2$ hydrogenation; plasma; dielectric barrier discharge; synergy; catalyst

1. Introduction

With economic development, industrialization, and human activity, the continuous increasing emission of CO$_2$ has led to the increase of global temperature (i.e., global warming) which has an impact on the earth's ecological environment, such as glacier melting and sea level rise [1,2]. One way to reduce the CO$_2$ content in the atmosphere is to capture it with adsorbents (e.g., basic solvents and active carbons) [3]. However, major concerns regarding CO$_2$ capture and storage lie in separation efficiency, operation costs, and long-term stability [4,5]. In comparison, transformation of cheap and abundant CO$_2$ to value-added products (e.g., CH$_4$, CH$_3$OH, C$_2$–C$_4$ hydrocarbons) via hydrogenation has drawn tremendous attentions [1,6–23]. In some works, CO$_2$ splitting (dissociation) and reversed water–gas shift (RWGS) are considered a kind of hydrogenation process; however, a reaction involving both C–O bond breaking and C–H bond formation will be mainly covered in this review, such as methanation (Equation (1)) and methanol production (Equation (2)). Notably, CO$_2$ dissociation and RWGS might be discussed as an intermediate step or side reaction as well.

$$CO_2 + 4H_2 \leftrightarrow CH_4 + 2H_2O \quad \Delta H_{298K} = -252.9 \text{ kJ}\Delta\text{mol}^{-1} \quad (1)$$

$$CO_2 + 3H_2 \leftrightarrow CH_3OH + H_2O \quad \Delta H_{298K} = -49.5 \text{ kJ}\Delta\text{mol}^{-1} \quad (2)$$
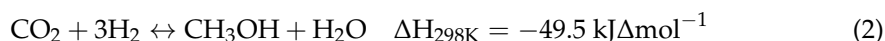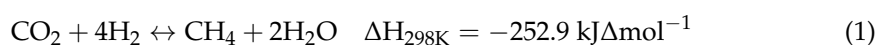
The possible reaction mechanisms of various hydrogenations of CO$_2$ are as below (Figure 1a,b). Obviously, based on their exothermic nature, these processes are thermodynamically favored at low temperatures; however, considering the eight-electron reduction

of CO_2 and activation of H_2, a catalyst is necessary for the activation of CO_2 and H_2 to enhance the reaction kinetics [24]. Moreover, intensive conditions are necessarily applied to realize the industrial applications in conventional thermal catalysis. For example, in methanol production, a temperature of 200–300 °C and high pressure of 3–30 MPa are usually required [1,25–28]. Coupling with non-thermal plasma (NTP), especially dielectric barrier discharge (DBD)-generated plasma can form a synergy where both a mild reaction condition and high selectivity are achieved (Figure 1c). Specifically, the electric field can be enhanced by the catalyst and micro-discharges can be generated in the pores; on the other hand, the catalyst physicochemical properties and reaction pathways could be changed in the presence of plasma and an easier activation of reactant molecules is enabled [29–36]. In the plasma–catalyst hybrid system, a high conversion efficiency and selectivity can be obtained at a relatively milder reaction condition. For example, when Ru/Al_2O_3 was combined with DBD plasma, 12.8% CO_2 conversion and 73% CH_4 selectivity were delivered in methantion of CO_2 at only 25 °C [37]. While in the production of CH_3OH, the combination of DBD plasma and $CuO/ZnO/Al_2O_3$, the optimal reaction temperature was lowered by 120 °C compared with the catalyst only approach [26]. Several reviews have been reported in plasma-assisted catalytic CO_2 conversions [1,2,6–8,29,38,39]; however, a comprehensive and in-depth summary is rarely seen regarding the synergistic effects of catalyst–DBD plasma hybrid system on the catalytic performances and energy efficiency of CO_2 hydrogenation. In the following sections, an overview of the plasma (particularly DBD plasma) and a detailed description of the synergy will be provided in terms of structure–performance relationships. Subsequently, the effects of operation parameters and reactor designs are illustrated, followed by possible reaction mechanisms of CO_2 hydrogenation in this hybrid system. In the end, conclusive remarks and future works are proposed.

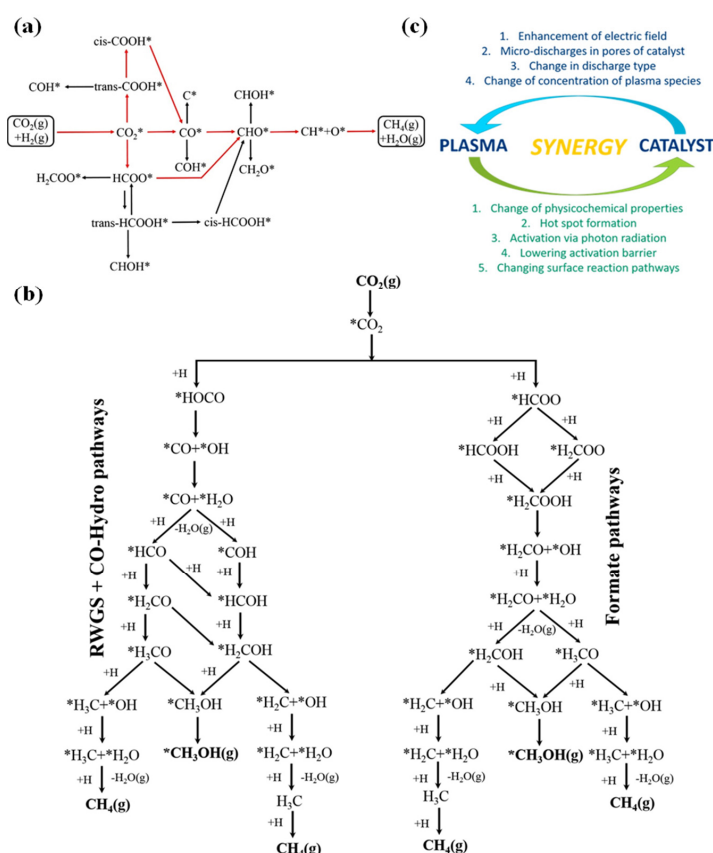**Figure 1.** Reaction pathways for (**a**) CO_2 methanation (preferred steps highlighted in red). Reprinted with permission from [40]. Copyright 2018 Elsevier. (**b**) CO_2 hydrogenation to CH_4 and CH_3OH. Reprinted with permission from [41]. Copyright 2016 Elsevier. (**c**) Synergy in plasma–catalyst system. Reprinted with permission from [29]. Copyright 2019 Elsevier.

2. Overview of Plasma and Catalyst–Plasma Hybrid System

As a chemical mixture of cations, anions, molecules, atoms, excited species, and radicals which interact with each other, plasma is widely utilized in many aspects of material science, microelectronic industry, environmental applications, and medical treatments [42]. Rather than natural plasmas, two man-made plasmas are mainly involved in research, that is, completely ionized plasmas (fusion plasmas) and weakly ionized plasmas (gas discharges) [6]. The gas discharges can be further classified into two types depending on if the plasma is in thermal equilibrium, which are thermal plasmas in local thermodynamic equilibrium (LTE) and non-thermal plasmas (NTP) in non-LTE conditions [6]. Thermal plasmas enjoy many advantages, such as high energy density, high radiation intensity, and high temperature. However, their applications in CO_2 conversions are limited by the lower equilibrium efficiency and conversion than NTP. To create the NTP, a gas-filled reactor is inserted by two electrodes parallel to each other, where an electric field is generated by applying a potential difference. Some gas molecules can be broken into cations and electrons, and the accelerated electrons will collide with the gas molecules on the way to the anode, leading to ionization, excitation, and dissociation. New electrons could be released from the produced ions in previous ionization collisions at the cathode, and these electrons enable further collision and resulting ionization. Owing to this self-sustaining non-thermal plasma, gas molecules would be activated by high-temperature electrons, creating radicals and products [6]. The major merits of NTP in CO_2 conversions include the following points. First, the high-energy electrons created by the plasma in an electromagnetic field can initiate the CO_2 activation even at ambient conditions without the thermal energy input to heat up the reactor or reactants. Second, the operation flexibility (ability to be instantaneously turned on and off) allows the NTP technology to adapt to the intermittent renewable energy [38]. Third, the low cost of plasma reactors without the usage of rare earth materials improves scalability in household devices, on-demand installations, and large-scale plants [43,44]. Among the various discharges applied to create NTP—such as gliding arc discharges, glow discharges, microwave discharges, and DBD [1,38]—DBD is widely studied due to the generation of highly active species and high electron density [39], facile design, and operation in ambient conditions [38]. In the representative DBD plasma reactor (Figure 2a), the grounded electrode in the center is surrounded by the coaxial dielectric tube covered by stainless steel mesh and powered by the high potential. For comparison, a planar DBD reactor is shown in Figure 2b, where the dielectric barrier materials are in contact with the two electrodes at the top and bottom side. Despite the highly active electrons which activate the gas molecules in mild conditions, an uncontrollable recombination of the intermediates occurs, lowering the targeted product selectivity. Even worse, the formed end-products can be further destroyed by the electrons. This scenario becomes more obvious in CO_2 hydrogenation which is more complicated than CO_2 splitting where CO and O_2 dominate the products [6]. Therefore, a catalyst is necessarily coupled in the DBD reactor to realize both a high selectivity and low energy input. In turn, the catalyst lifespan would be prolonged under mild conditions.
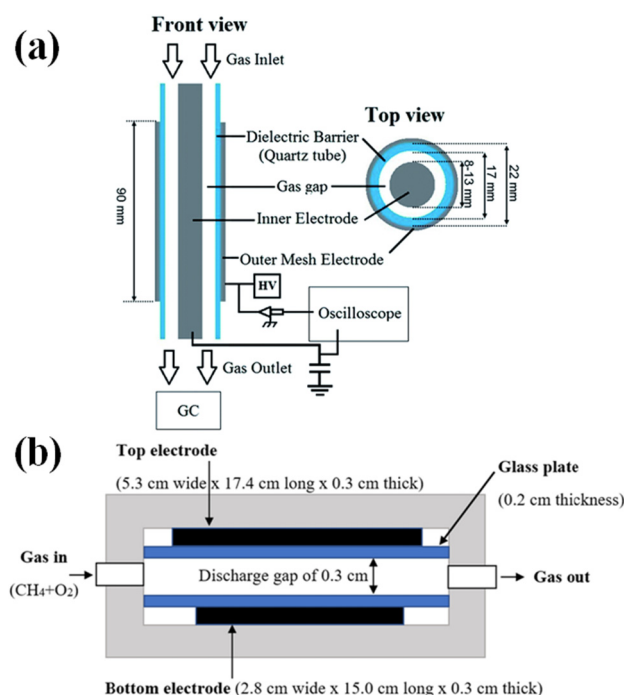
Figure 2. DBD plasma reactor: (**a**) Coaxial tube. Reprinted with permission from [38]. Copyright 2015 The Royal Society of Chemistry. (**b**) Plate-to-plate. Reprinted with permission from [45]. Copyright 2020 Springer.

In the catalyst-plasma hybrid system, prior to the adsorption on the catalyst surface, the CO_2 has become excited in the presence of DBD plasma, thus promoting the conversion to intermediates with a lower energy barrier than with thermal catalysis alone where a higher temperature is needed to activate the adsorbed ground-state CO_2 molecules [46,47]. Moreover, the surface reactions can be further facilitated due to the involvement of active species excited in the plasma—such as CH, OH, and CO radicals [48,49]. Furthermore, as previously mentioned, the interaction between catalysts and plasma would modify the surface properties of the catalysts (e.g., basicity, adsorption capacity) and the plasma characteristics [50–52]. In the following part, an in-depth and comprehensive discussion is provided regarding the applications of the above hybrid system in CO_2 hydrogenation and the corresponding structure–performance relationships.

3. Synergy in Catalyst–Plasma (DBD) Hybrid System

To realize the low-temperature and efficient conversion of CO_2 and high selectivity of targeted products via hydrogenation, the catalyst can be integrated with the DBD plasma reactor to generate a synergy, where the respective properties of active metals, supports, and promoters (additives) can be effectively combined.

3.1. Active Metal and DBD Plasma

When DBD plasma was applied in Pt/In_2O_3 catalytic CO_2 hydrogenation to methanol, a highly dispersed Pt nanoparticle was obtained, delivering a 37% CO_2 conversion and 62.6% methanol selectivity at 30 °C and 1 atm, much higher than that of conversional Pt/In_2O_3 (24.9% and 36.5%, respectively) (Table 1). This enhanced performance was mainly attributed to the stronger adsorption of CO_2 by small Pt nanoparticles (2.32 mmol/g) and lower energy barrier to initiate the hydrogenation in the presence of plasma [53]. Besides Pt, Pd is reported to be highly active in methanol production from CO_2 hydrogenation at low pressures [54]. When coupled with DBD plasma at a 30 W discharge power, CO_2 conversion increased from 17.1% to 32.5% due to the accelerated dissociation of gaseous and adsorbed CO_2 by plasma and strengthened adsorption of produced CO intermediate

on Pd surface [6,55]. With the increase of Pd loading from 0.69 wt% to 2.29 wt%, the conversion of CO_2 increased by almost 100%. As another representative noble metal, Ru has been proven active for CO_2 hydrogenation in previous studies with HCOO– as the intermediate [56]. Interestingly, Ru^{3+} could be in-situ reduced to Ru metallic phase, which exhibited a highly selective methanation via CO_2 hydrogenation [57]. The combination of DBD plasma and Ru enabled the successive deoxygenation of CO_2 and further conversion to CH_4 [37].

Table 1. Catalytic CO_2 hydrogenation assisted with DBD plasma.

Catalyst	Targeted Product	H_2/CO_2	CO_2 Conversion (%)	Selectivity (%)	Applied Voltage (kV)	Ref.
Pt/In_2O_3	CH_3OH	3	37	62.6	13.3	[53]
$Co/CeZrO_4$	CH_4	4	70	100	20	[52]
Co/ZSM-5	C_2-C_4	3	45	13.7	10	[58]
Ni/Al_2O_3	CH_4	4	60	97	10	[47]
Co/Al_2O_3	C_2^+	3	74	46.5	18.5	[59]
Ni/UiO-66	CH_4	4	85	99	6.5	[60]
CeNi/Cs–USY	CH_4	4	70	95	6	[61]
$Ni-CeO_2/Al_2O_3$	CH_4	4	70	96	7.7	[62]
Ni–La/Na–BETA	CH_4	4	85	97	6	[63]
Ni–Fe/LDH	CH_4	4	72	99	18	[64]
$Ni-Na/CeZrO_x$	CH_4	4	57.5	75.9	15	[65]

In addition to noble metals, various transition metal catalysts have been widely studied as alternatives considering their low cost and high activity. Cu-based catalysts exhibit superior intrinsic activities towards methanol production from CO_2 hydrogenation [66–69]. Compared with Pt, Cu delivered a better performance owing to the moderate adsorption of oxygen species and bonding with the intermediates, despite the larger particle size than Pt [70]. When integrated with DBD plasma, a high methanol selectivity of 53.7% was achieved due to the simultaneously promoted adsorption and activation of CO_2 and conversion to CH_3OH. In another work, however, the addition of Cu caused a lower conversion of CO_2 resulting from the increased ionic conductivity and reduced dielectric constant, which enhanced the voltage needed for plasma ignition [71]. By replacing Cu with Mn, the energy efficiency was improved by 116% in DBD reactor (1620 µg/kJ). Moreover, CO_2 conversion was increased by 36% with DBD plasma [72]. Notably, when Cu and Mn were coupled, the side reaction WGS was inhibited and a facilitated formation of carbonate species as a result of CO_2 adsorption was observed on the catalyst surface [73].

Compared with Cu which binds strongly with CO_2 and CO, Co is more selective to produce CH_4 [24,74,75]. At the Cu surface, adsorbed carbonates and formates decomposed to form certain amount of CH_4; however, the main products were still CO derived from the RWGS of CO_2 even with plasma. On the contrary, the CH_4 selectivity was significantly increased from 25% to 88% at the Co surface with the help of DBD plasma (Table 1). In particular, triggered by the plasma electronic impact collisions, the gaseous CO dissociated from CO_2 was re-adsorbed onto the surface of Co metals, which further dissociated to O and C, subsequently reacting with the H atoms simultaneously generated from H_2 molecule decomposition to form CH_4. Owing to the inherent positive contribution of DBD plasma and Co metallic sites, the temperature to reach the maximum CH_4 yield was reduced by 40 °C [52]. In another scenario where the DBD plasma voltage was 13.6 kV, furnace temperature was 250 °C and H_2/CO_2 was 3, CO_2 was selectively converted to CH_4 on Co surface; interestingly, CH_x species formed in plasma were immediately terminated by the H species also produced in plasma, leading to a dominant amount of CH_4 and only a trace amount of longer-chain hydrocarbons [59]. Lan et al. [58] further compared a series of active metals in DBD plasma–catalytic production of CH_4 and lower hydrocarbons via CO_2 hydrogenation. With an input power of 14 W and H_2/CO_2 ratio of 3, Co was proven more active than Cu, Fe, and Mo in terms of the CO_2 conversion and hydrocarbon

selectivity. In detail, over 40% conversion of CO_2 was achieved in Co catalyst while those of the counterparts were only less than 20% (Table 1). Moreover, the CH_4 selectivity of Co catalysts reached more than 70% while those of other metals were lower than 20%. These enhanced conversions of CO_2 to hydrocarbons were attributed to the synergistic effects of metals and plasma; specifically, the CO and H species produced in plasma were adsorbed at the metal surface where CO methanation was highly activated, contributing to the formation of CH_4 and CH_x products [76].

Similar to Co, Ni is also proven effective in CH_4 production via CO_2 hydrogenation [58]. When coupled with plasma, over 80% CO_2 conversion and 99% CH_4 selectivity can be achieved at low temperatures [77]. In another situation at 150 °C and 10 kV voltage, the Ni/Al_2O_3–DBD plasma hybrid system realized 60% CO_2 conversion and 97% CH_4 selectivity, increasing by 20 and 5 times in comparison to plasma alone (Table 1) [47]. After the reaction, the Ni size and dispersion was 6.3 nm and 42% in plasma respectively, better than that in thermal catalysis (8.1 nm and 24%) (Figure 3a), which was ascribed to the immediate capture of O radicals from CO_2 dissociation by the active H species to form OH and CHO radicals in plasma (Figure 3b) [37,78]. Rather than the smaller size and higher dispersion, the stabilized metallic Ni phase by excessive electrons and strong reducibility under plasma discharge was more crucial in this case [79]. The electron transfer over the Ni^0 surface promoted the bond breaking and formation, pushing the forward reaction and enhancing the catalytic conversion and selectivity [79,80]. Besides the metallic Ni effect, the redox property and Lewis basic sites were improved due to the surface electrons, promoting the CO_2 adsorption which is a Lewis acid (Figure 3c) [79,81]. Moreover, the dissociation of CO_2 was facilitated when they were activated by plasma to form vibrational and excited states, intrinsically accelerating the CO production in a lower energy barrier [82]. The improved CO_2 activation could be signaled by the production of CO_2^+, CO, CHO radicals, and C_2^- species; and the last two species were mainly responsible for the high conversion to CH_4 with surface-bound H at low temperatures in Ni/Al_2O_3 coupled with DBD plasma [83–85]. Interestingly, the insignificant enhancement of temperature (170 °C at the outlet and 150 °C at the reaction zone) and zero carbon formation excluded the overheating of bed materials by the plasma (thermal effect) or the resulting hotspots. Thus, the dominant driving force of the excellent activity was the stimulation by the high-intensity microdischarges in-between the reactor and beads, together with a new reaction pathway [86,87].

In a few other studies, however, the Ni particle size effect on the performance and the influence of plasma on the Ni size were emphasized. In Ni/Zeolite catalyst with DBD plasma for CO_2 methanation, the CO_2 conversion was greatly enhanced from 15% to 95% compared with catalyst alone since various reactive species produced by the plasma contributed to the C–O dissociation which determined the reaction rate in CO_2 hydrogenation. Moreover, the highly dispersed and small Ni nanoparticles further increased the conversion efficiencies [88]. To further explore the effect of Ni dispersion and location on the CO_2 conversion and CH_4 selectivity, Ni supported or encapsulated in silicalite-1 with various pore structures were tested in DBD plasma reactor [89]. Notably, those Ni active sites at the external surface of silicalite-1, or embedded in the hierarchical pore structures, exhibited better performances than those in microporous structures, which could be explained by the facilitated diffusion of short-lived reactive species generated in plasma (e.g., radicals and excited atoms/molecules) and high exposure of active centers where the possible deactivation of plasma-induced species was inhibited [90,91]. Apart from the effect of Ni size on the catalytic activity, the presence of DBD plasma relates strongly with the generation of Ni nanoparticles with different sizes. It is reported that less defective and smaller Ni sites were formed when interacting with the plasma [92]. Owing to the activation of DBD plasma, Ni dispersion was improved considerably and the resulting Ni particle size was only 4 nm in average, much smaller than that obtained in thermal catalysis (13 nm) [60]. More interestingly, when plasma was applied in the pre-treatment of Ni nitrate precursors, one-step reduction to Ni^0 phase was realized in a fast decomposition rate, where the diffusion of Ni species into the $MgAl_2O_4$ support pores was alleviated, thus obtaining a

weak metal–support interaction and better reducibility. Additionally, the nucleation and crystal growth of Ni were modified in the plasma. The formed abundant Ni active sites effectively catalyzed the methanation of CO as an intermediate derived from the formate decomposition [93].
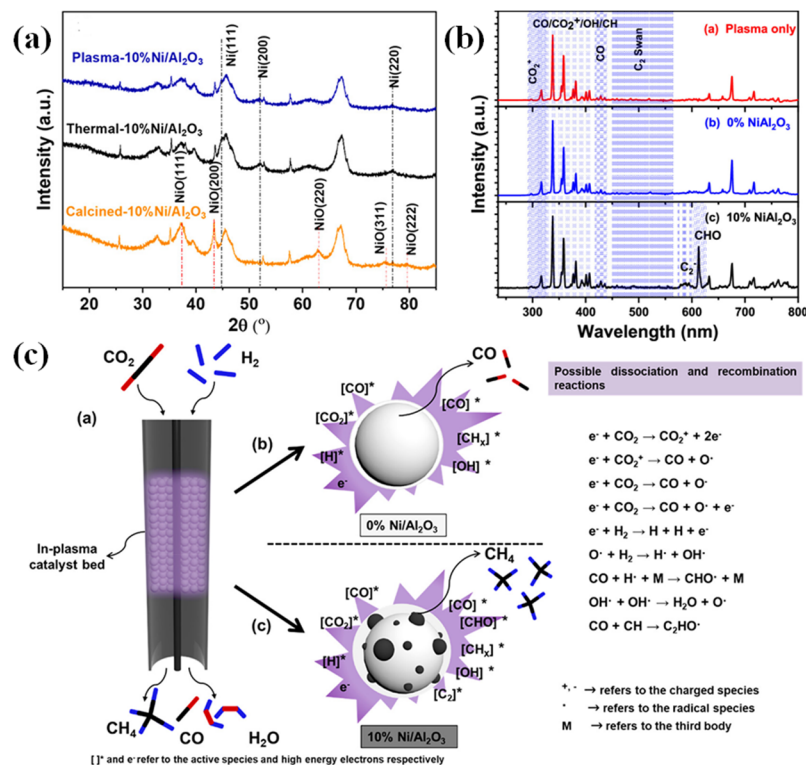

Figure 3. Characterization and reaction pathway of the catalyst: (**a**) XRD patterns, (**b**) OES spectra, and (**c**) proposed reaction scheme of Ni/Al_2O_3 catalysts in different reaction conditions. Reprinted with permission from [47]. Copyright 2020 American Chemical Society.

3.2. Support and DBD Plasma

In the presence of DBD plasma, high energy species in abundance can be generated, thus lowering the activation energy and reaction temperature [71]. It is noteworthy that the catalyst itself may change the plasma properties, including micro discharge generation in the pores, discharge type modification, and electric field enhancement [94]. In addition to particle size (a small size usually requires a higher ignition voltage), the intrinsic properties of support materials (e.g., dielectric constant and ionic conductivity) determine the energy of plasma in a way that a high dielectric constant and low conductivity benefit a strong capability to store energy [71]. When Al_2O_3 was introduced to the DBD reactor, the dielectric constant was enhanced owing to the non-conductivity of Al_2O_3, leading to an increased energy of the ionized electrons at a lower breakdown voltage [86,95–97]. Benefiting from the denser plasma, reactive radicals and intermediates accelerated the transformation of CO to HCO^* and $HCOO^*/H_2CO^*$, contributing to the methanol production with a higher TOF [71]. In another scenario where C_2^+ hydrocarbons were the targeted products, the Al_2O_3 packing in the DBD reactor promoted the chain-growth reaction of CH_x derived from the activation of plasma. Additionally, when the input power increased to 10 W from 4 W, 74% CO_2 conversion and 46.5% C_2^+ selectivity were delivered at 25 °C (Table 1) [59].

Apart from Al_2O_3, transition metal oxide ZnO is proven effective in CO_2 hydrogenation assisted with DBD plasma. The partially reduced ZnO_x possessed abundant oxygen vacancies, increasing the amount of medium CO_2 activation [98,99]. Meanwhile, the desorption temperature was reduced in the presence of plasma [100]. On the other hand, the addition of ZnO enabled a lower ionic conductivity and higher dielectric constant,

thus generating a denser plasma which benefited the CO_2 dissociation via electron impact activation [101].

Different from ZnO, $CeZrO_2$ is featured with the superior redox property and oxygen storage capacity, acting as a reservoir of CO^* and O^*, which were the dissociation products of CO_2 [88]. Accelerated by the plasma, the decomposition of adsorbed species and recombination with H to form CH_4 were favored at 90 °C, delivering a high CO_2 conversion of 80% and 100% CH_4 selectivity. Moreover, the intrinsic basicity was well maintained after 100 h activity test based on the CO_2-TPD results, suggesting a stable adsorption of CO_2 during the CO_2 methanation catalyzed by $Ni/CeZrO_2$ and plasma. In comparison, much lower CO_2 conversion (5%) and CH_4 selectivity (0%) were obtained in plasma alone [102]. Parastaev et al. [52] applied temperature-programmed plasma surface reaction method to further study the role of $CeZrO_4$ in CO_2 hydrogenation, where CO_2 was adsorbed on the catalyst followed by feeding H_2 with a ramping temperature in a tubular DBD reactor. A higher temperature might be detrimental to the CH_4 yield due to RWGS side reaction. For example, more CO but less CH_4 was produced above 275 °C and only a negligible amount of CH_4 was observed at 400 °C [52]. The synergy of $CeZrO_4$ and plasma was proposed based on the results that CO_2 adsorbed on the $CeZrO_4$ to form formate and carbonate species; under the plasma-induced electron impact dissociation, CO was generated and subsequently reacted with the reactive H^* species to form CH_4 [103,104]. As previously mentioned, CO_2 adsorption was facilitated at the basic sites of $CeZrO_x$. Notably, despite no general agreement, low- and medium-strength basic sites are possibly preferred for the methanation compared with strong ones [105]. Interestingly, after pre-treatment in DBD plasma for an excessive duration (i.e., 60 min), the concentration of strong basic sites were increased, which adversely reduced the CO_2 conversion. With a shorter treatment time (i.e., 40 min), 80% CO_2 conversion was delivered at a low input power of 5 W, much smaller than 13 W power for the thermally calcined counterpart [78].

As a porous material, zeolites are a proven efficient support for CO_2 hydrogenation due to the marked influence of the framework on performances [58]. When ZSM-5 was packed on the DBD reactor, the CO_2 conversion was increased to 25% from 8.1% without packing. This enhanced performance was attributed to the synergy between ZSM-5 and DBD plasma. In particular, O and H atoms produced via the plasma-induced electron impact dissociation were anchored on the ZSM-5 surface; meanwhile, the electrons might be trapped in the pores of ZSM-5. Therefore, the lifetime of the active species (e.g., H and O) was considerably prolonged owing to the weak chemisorption, and surface streamers were generated from the trapped electrons acting as the reservoir. In addition to the promoted interaction with the active species for CO_2 hydrogenation, the immediate water removal was realized on the zeolite surface in the plasma, promoting the adsorption/activation of CO_2 and alleviating the negative effect of H_2O on the methanation [61].

Owing to the outstanding adsorption capability of CO_2, Zr-MOF exhibits great potential in CO_2 hydrogenation [57]. Moreover, the high surface area and abundant surface hydroxyl groups benefit the dispersion of active metals [106–108]. In the presence of non-thermal plasma, the structure of Zr-MOF is effectively stabilized even under water [109,110]. However, after thermal calcination, the collapse of MOF structure probably occurred. These assumptions could be confirmed by the XPS results that, for the plasma-treated Zr-MOF, only the carboxylate and hydroxylated species in Zr-MOF (UiO-66) appeared without change in the Zr 3d spectra [111]; however, formation of $O–Zr^{4+}$ and Zr–O signified the decomposition of the MOF structure under calcination (Figure 4a–d) [112]. The intact MOF support was also reflected by the morphology in TEM image (Figure 4e), ensuring a highly dispersed Ni active site. Furthermore, the hydroxyl groups generated in the plasma-treatment benefited the CO_2 adsorption. Owing to the above merits, the plasma-treated Ni/UiO-66 catalyst exhibited a fairly stable CO_2 conversion (85–90%) over 20 h, outperforming that in thermal catalysis at 380 °C (Figure 4f) (Table 1) [60].
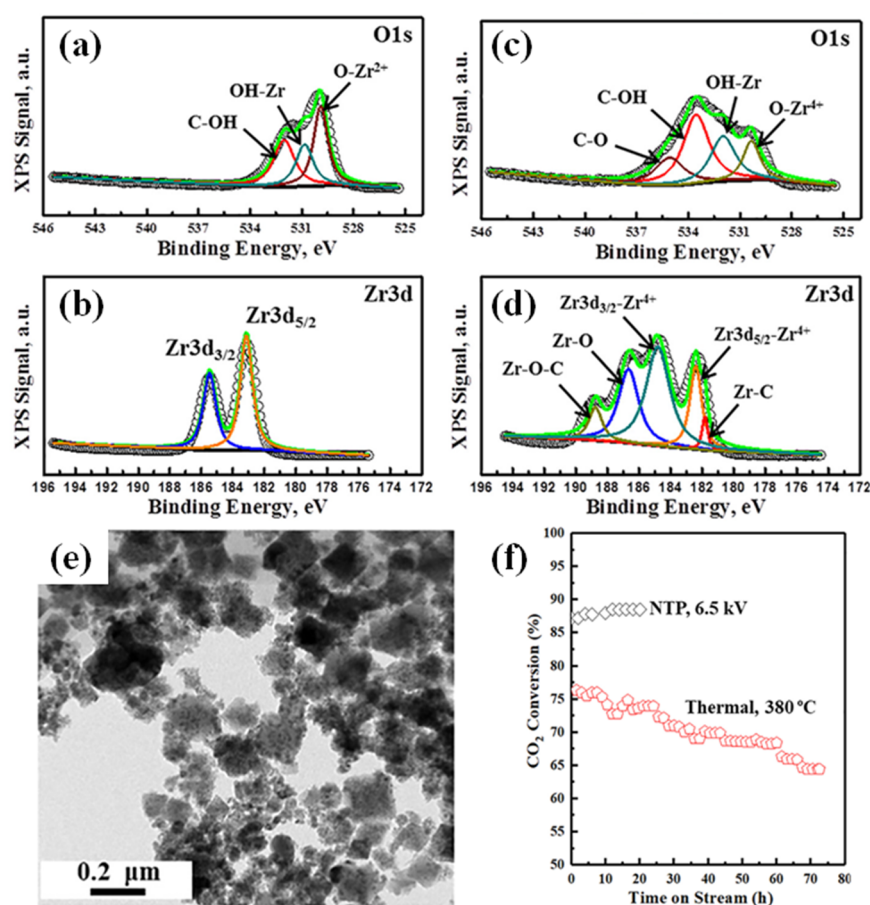
Figure 4. Characterization and stability test of the catalysts: XPS spectra of spent Ni/UiO-66 catalyst activated in DBD plasma (**a**) O 1s (**b**) Zr 3d and thermally calcined (**c**) O 1s (**d**) Zr 3d. (**e**) TEM image of spent Ni/UiO-66 activated in DBD plasma. (**f**) Stability test of Ni/UiO-66 catalyst activated in DBD plasma and thermally calcined (CO_2 conversion). Reprinted with permission from [60]. Copyright 2020 Wiley.

3.3. Additive and DBD Plasma

Featured with the improvement of pore volume and surface area, CeO_2 is widely adopted as an additive in metal-based catalysts [113]. More interestingly, CeO_2 with a high dielectric constant ($\varepsilon_r = 24$) is able to change plasma property by adjusting the electron impact reaction kinetics since the charge accumulation and polarization effect enable an enhanced electric field [87]. Thus, a high CO_2 conversion of 70% and CH_4 selectivity of 95% were obtained at 5–6 kV voltage and H_2/CO_2 ratio of 4 (Table 1) [61]. In addition to the modification of plasma, owing to the moderate basic sites, CeO_2 as an additive can adsorb CO_2 to form carbonates, which are further reduced to formates and formaldehydes, subsequently generating CH_4 as the end product [104,114]. When coupled with DBD plasma, CO_2 molecules were first activated to CO_2^*, thus lowering the reaction temperature. According to Figure 5a, both Ni/Al_2O_3 and $Ni/CeO_2–Al_2O_3$ treated in plasma possessed larger CO_2 desorption peaks than the thermally calcined ones, indicating more abundant basic sites generated by plasma. Moreover, the larger desorption peak between 200 and 350 °C for $Ni/CeO_2–Al_2O_3$ suggested a higher concentration of medium basic sites, which were mainly responsible for the CO_2 adsorption and activation [115]. More significantly, the methanation of CO as an intermediate of plasma-stimulated CO_2 dissociation preferentially took place at CeO_2 when the loading of CeO_2 was lower than 10% [116]. A higher CeO_2 content would adversely affect the CH_4 yield due to the negative texture effects and unfavorable interaction with basic CO. Benefiting from the synergy of DBD plasma and CeO_2, a high yield of methane (80%) was achieved at 150 °C while only

60% CH_4 was obtained at 400 °C for thermal catalysis [62]. Apart from the modification effect on the surface basicity, the electron transfer environment could be created resulting from the unique redox property of CeO_2, leading to the CO_2 adsorption [117]. In detail, oxygen vacancies could be generated based on the loss of oxygen when exposed to plasma. Subsequently, CO_2 adsorbed onto the surface by fulfilling the vacant sites, facilitating the activation of CO_2 via electron impact dissociation [118]. As shown in Figure 5b, the second reduction peak of Ni/CeO_2–Al_2O_3 treated in plasma signified the partial reduction of Ce^{4+} to Ce^{3+} [119]. Importantly, CO_2 preferentially adsorbed onto the oxygen sites next to Ce^{3+} and the activated CO_2 on Ce^{3+} was more easily hydrogenated [10–35], thus delivering a high CO_2 conversion of 63% and CH_4 selectivity of 96% at 250 °C [120]. Again, an appropriate addition of CeO_2 might contribute to the oxidation of surface dissociated carbon to form CO species; however, an excessive amount of CeO_2 possibly initiated the further combination with O to produce CO_2 again, lowering the CO_2 conversion and hydrogenation efficiency [121].
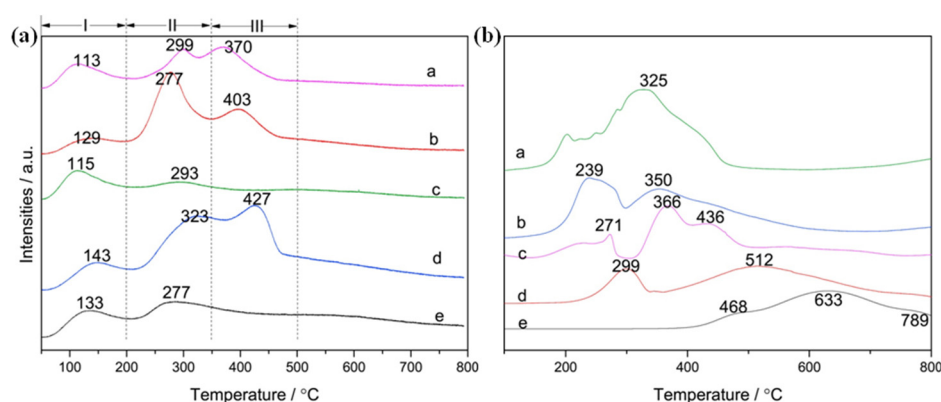

Figure 5. Characterization of the catalysts: (**a**) CO_2-TPD and (**b**) TPR profiles of a: Ni/Ce-p, b: Ni/CeAl-p, c: Ni/CeAl-c, d: Ni/Al-p, e: Ni/Al-c. Reprinted with permission from [120]. Copyright 2015 Elsevier.

As another rare earth metal oxide, La_2O_3 is also a proven effective additive to enhance the catalytic performance of CO_2 hydrogenation in DBD plasma. When La_2O_3 was incorporated in the Ni/BETA zeolite applied for CO_2 methanation, 85% CO_2 conversion and 97% CH_4 selectivity were obtained below 150 °C, while for the conversional thermal activation, only 80% CO_2 conversion was achieved at 400 °C (Table 1). Moreover, the 15-h stable activity suggested a robust catalyst under DBD plasma [63]. This excellent catalytic performance of Ni/La_2O_3–BETA zeolite was ascribed to the synergy between the plasma and La_2O_3 additive. Specifically, more hydroxyl groups were generated with the introduction of La_2O_3, strengthening the adsorption of CO_2 and preventing the gaseous CO_2 from being dissociated by plasma [122,123]. On the other hand, only carbonates were formed via thermal activation; in comparison, apart from the carbonates, monodentate formates were also generated on the La_2O_3 in the presence of DBD plasma, which were easily hydrogenated to CH_x species, thus leading to a high yield of CH_4 [116,123].

Characterized with the promotional effect on the reducibility and dispersion of Ni, the coupling of Ni with Fe increases the active site concentration of Ni-based catalyst [64]. When Ni–Fe LDH was combined with DBD plasma in CO_2 methanation, 75% CO_2 conversion and 97% CH_4 selectivity were obtained at 250 °C and an input power of 11.7 W (Table 1) [64]. On one hand, the energy utilization efficiency was enhanced in the DBD reactor, thus saving energy and lowering the reaction temperature without heating the reactor [78,105]. On the other hand, both weak and medium basic sites were increased with the addition of Fe, benefiting the CO_2 adsorption. Under plasma, CO_2 dissociated into CO, followed by forming formates and linear carbonyls, which were further hydrogenated into CH_4 [116].

Besides the rare earth and transition metal oxides, alkali metals (e.g., Na and K) are also doped into the Ni-based catalysts owing to their strong basicity. However, they were

proven to cause a negative influence on the physicochemical property of $Ni/CeZrO_x$ and reduction of performances in CO_2 methanation assisted with DBD plasma [65]. In detail, owing to the molten salt effect, a larger $CeZrO_x$ particle size with less defects was produced, lowering the cycling rate of Ce^{3+}/Ce^{4+} and oxygen vacancy concentration, reflected from the higher temperature reduction peaks in TPR profiles (Figure 6a). Additionally, the overly basic sites generated in the presence of Na and K impeded the participation of adsorbed CO_2 in the next-step reaction by formation of bridged and polydentate carbonates [124], as shown in the high temperature desorption of CO_2 in Figure 6b. Furthermore, despite the considerably enhanced dielectric constant in Na- and K-promoted catalysts, the excessively low breakdown voltage and intense ionization accelerated the direct CO_2 splitting into CO rather than further hydrogenation of the intermediates, resulting in a decrease of CH_4 yield and a higher power consumption (Figure 6c). Compared with the undoped $Ni/CeZrO_x$, the Na- and K-doped samples exhibited a 16–17% reduction of CO_2 conversion, 23–31% decrease of CH_4 selectivity, and 7–8 W increase of power input [65].
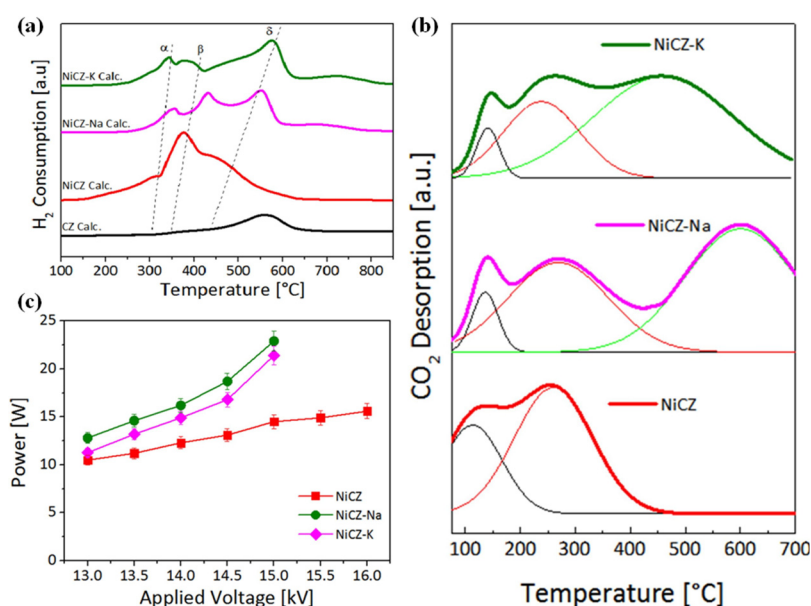

Figure 6. Characterization of the catalysts: (**a**) H_2-TPR, (**b**) CO_2-TPD, and (**c**) average power dissipated against the voltage for calcined catalysts. Reprinted with permission from [65]. Copyright 2021 Elsevier.

Apart from the metal additives, the introduction of Ar gas was proven to be influential for the reaction pathways and CO_2 conversion for Ni/Al_2O_3 catalyst assisted by DBD plasma [55]. In detail, the breakdown voltage was lowered from 3.1 to 2.6 kV with an increased amount of Ar from 0% to 50% due to less attachment of free electrons on CO_2 molecules and reduced dielectric strength of working gas [125]. Moreover, the addition of Ar promoted the Ni–DBD plasma interaction, thus realizing a sufficient contact during the reaction. Furthermore, Ar gas changed the discharge mode 'partial discharging' to 'fully-bridged' discharge, injecting more power into the reaction instead of being deposited on the dielectric surface, leading to a higher energy efficiency and effective capacitance. As a result, with the Ar feed increasing from 30% to 60%, the CH_4 selectivity was enhanced from 42% to 100% at 150 °C. More interestingly, the generated metastable argon (Ar^*) facilitated the dissociation of CO_2 and H_2 into C, O, and H atoms which further recombined at the catalyst surface to form targeted product CH_4 [55].

4. Operation Parameter

In addition to the catalyst design, the operation parameters considerably affect catalytic performances in CO_2 hydrogenation in catalyst–DBD plasma hybrid system, including the voltage, power, temperature, pressure, feed ratio, and GHSV [26,49,58].

4.1. Voltage/Power/Temperature/SIE (Specific Input Energy)

As usual, a high voltage generates a high power and temperature in the reactor. A series of voltages were applied in the $Ni/CeZrO_2$ catalyst for plasma catalytic CO_2 methanation (Figure 7) [49]. The highest CO_2 conversion and CH_4 selectivity was achieved at 16 and 15 kV respectively. Correspondingly, the power generated was between 20 and 40 W and the temperature reached the range of 230–270 °C. The enhanced performance at 15–16 kV compared with 14.5 kV was probably due to the promoted CO_2 adsorption and dissociation in a stronger electric field with micro-discharges in the bed materials [126–128]. A further increase of the applied voltage (e.g., 18 kV) caused an adverse effect on the performance that an obvious drop of CH_4 was shown from 100% to 82%, which might be related to the higher temperature generated at a higher voltage, benefiting the endothermic RWGS reaction and thus producing more CO instead of CH_4 [104,129]. Similarly, in methanol production by combined Pt/In_2O_3 and DBD plasma, the best performance was obtained at 30 W power; a further increase of the power would reduce the CO_2 conversion and CH_3OH selectivity due to the dissociation of CH_3OH back to CO_2 and H_2O [53]. In another research based on the zeolite catalysts, however, a higher CH_4 selectivity was favored at a higher input power [61]. A possible explanation was that a low power might not be able to further convert the CO to CH_4, while a high power could sufficiently push the methanation process and producing a dominant amount of CH_4. In terms of the production of C_2–C_4 hydrocarbons, a high input power was probably required based on the simultaneous decrease of CH_4 but increase of C_2–C_4 hydrocarbons selectivity [58], which might signify the further conversion of CH_4 to longer-chain products under a stronger electric field and intensified electron collisions. Above all, appropriate selection of the applied voltage (power) based on the specific situation is probably needed to balance between the effective activation and inhibition of side reactions. Notably, SIE (ratio of power to flow rate) increases with the increase of applied voltages at a constant flow rate; thus, in most cases, the SIE and voltages exhibit a similar effect on the performances [130].
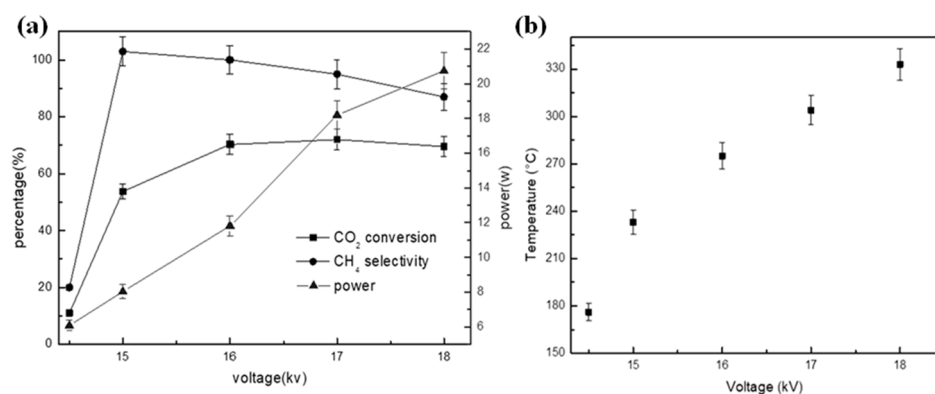

Figure 7. Activity test and voltage impact for the catalysts: (**a**) CO_2 conversion, CH_4 selectivity and power against the voltages. (**b**) Temperature against the voltages. Reprinted with permission from [49]. Copyright 2019 Springer.

4.2. GHSV (Gas Hourly Space Velocity)

As a ratio of the flow rate to the catalyst volume, GHSV is inversely proportional to the contact time [49]. Generally, in conversional thermal catalysis, a lower GHSV increases the CO_2 conversion due to the longer residence time of reactant on the catalyst surface [131]. In the presence of plasma, however, a higher flow rate and smaller catalyst mass enable a higher input power, thus intensifying the ionization process and generation of reactive species [132]. The relationship between GHSV and the temperature was further discussed depending on the magnitude of input power [133]. When the power was low (<10 W), temperature was independent from the GHSV since the plasma discharge was mainly responsible for the heat release; when the power was higher than 10 W, the heat produced from the exothermic reaction would not be ignored and the temperature increased with the

increase of GHSV owing to the larger number of CO_2 converted to CH_4 in unit time [133]. However, in terms of the conversion of CO_2 based on the percentage, there was a nearly 10% drop with a 3.5-fold higher GHSV, indicating the effect of contact time. In terms of competitive production of CH_4 and CH_3OH, the yield of CH_3OH was not sensitive to the GHSV but a sharp drop of the CH_4 selectivity was seen with the increase of flow rate [26]. In another case, the production of C_2–C_4 hydrocarbons (rather than CH_4 or CH_3OH) was gradually reduced with the increase of GHSV, indicating the necessity of a relatively longer residence time to ensure the chain-growth reactions [58].

4.3. Feed Ratio

The H_2/CO_2 feed ratio exerts a profound impact on the CO_2 conversion and product selectivity. For Co/ZSM-5 catalyst in DBD plasma, the CO_2 conversion and CH_4 selectivity showed a monotonic increase with the feed ratio increasing from 1 to 4. In comparison, the selectivity of C_2–C_4 hydrocarbons reached the maximum value at a ratio of 3 [58]. It might be reasonable since more H atoms generated in a high feed would convert more CO_2 to CH_4; however, an excessive amount of H_2 may adversely affect the C–C coupling process due to the competitive hydrogenation reaction. As for the methanol production, a relatively higher concentration of CO_2 (above 50% in the mixture of CO_2 and H_2) favored a higher selectivity of CH_3OH against CH_4; on the contrary, 10% CO_2 feed only delivered a low methanol yield (14%), 2.5-fold less than that of CH_4 [26]. This was probably in line with the previous finding that CH_4 was preferentially formed in the presence of abundant H_2.

5. Reactor Configuration

In previous sections, two basic configurations of the DBD reactors—coaxial and plate-to-plate type—have been introduced. In addition, the reactor can also be differentiated based on the location of catalysts. In particular, the reactor where the catalyst was placed downstream was called a 'two-stage configuration', while the reactor where the catalyst was loaded inside the discharge zone was called a 'one-stage configuration'. Obviously, only the long-lived species generated in the plasma could interact with the catalyst in two-stage mode. In one-stage configuration, the catalyst was exposed to more short-life species (e.g., radicals and electrons), leading to a different reaction pathway and performance [49]. In the following section, another few advanced reactor designs will be demonstrated to elaborate the influences on the catalytic performances and energy efficiencies in CO_2 hydrogenation.

As shown in Figure 8a, two types of DBD reactors differed in terms of their operation mode. Compared with the left pseudo-adiabatic one, the right adiabatic reactor was thermally insulated by granular spheres filled in a metal box [133]. Benefiting from the alleviated heat loss, the CO_2 activation was initiated at 5 W, half of the power needed in pseudo-adiabatic mode. Additionally, the maximum CO_2 conversion was achieved at 12.5 W in adiabatic conditions, again half of that in the pseudo-adiabatic conditions. Clearly, the thermal insulation effectively kept the inside temperature thus saving the power input and increasing the discharge transfer rate. At a 75% CO_2 conversion, the 58% energy efficiency (62 kJ/mol) was obtained in adiabatic reactor, 20% higher than that of the counterpart [133].

Different from the thermal insulation strategy to save the energy, SAPO membrane was integrated with the DBD plasma reactor to realize a simultaneous capture and utilization of CO_2 at a high efficiency (Figure 8b) [134]. As a kind of silico aluminophosphate zeolite, SAPO material was manufactured into a highly CO_2-selective membrane considering the appropriate pore size and strong CO_2 affinity [135,136]. When the membrane separation was coupled with the DBD reactor in CO_2 hydrogenation, 91.8% CO_2 capture efficiency and 71.7% CO_2 conversion efficiency were realized with a stable operation over 40 h. Notably, two-membrane system exhibited a 3.7-fold lower flow rate than the single-membrane separator, leading to nearly twice the efficiency for CO_2 capture and a 20% increase of CH_4 selectivity [134].
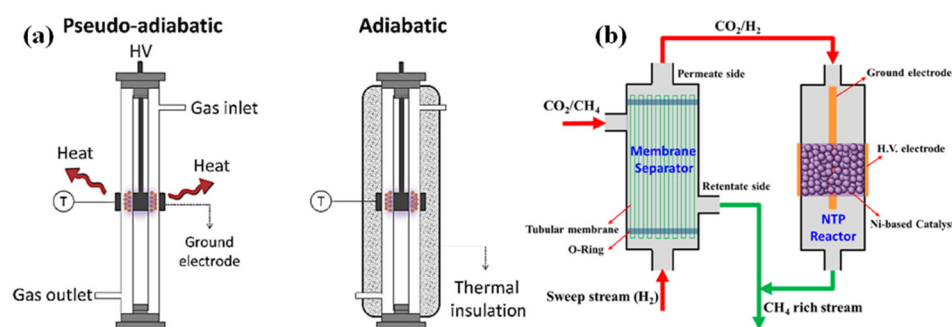
Figure 8. Various reactor designs: (**a**) Reactor configuration: (**left**) pseudo-adiabatic and (**right**) adiabatic. Reprinted with permission from [133]. Copyright 2020 Elsevier. (**b**) DBD reactor integrated with membrane separator. Reprinted with permission from [134]. Copyright 2020 American Chemical Society.

6. Reaction Mechanism

A deep and clear understanding of the reaction mechanisms benefits the effective control of the operation parameters, catalyst compositions, and reactor designs to ensure an optimized catalytic performance and energy efficiency in CO_2 hydrogenation. Several discussions on the proposed mechanisms will be presented as below.

By simulation with two-dimensional fluid model, CO_2 hydrogenation to CH_3OH was analyzed in terms of the detailed mechanism. Dominant reaction pathways included the electron-impact dissociation of H_2 and CO_2 to produce H, CO, and O radicals, followed by the recombination of H and CO to form key intermediate CHO. After successive hydrogenation by H atoms, CH_3OH was finally generated by the reaction of CH_3O and H, which was deemed as the major route. It is noteworthy that with the increase of H2 feed, the concentration of H_2O^+, O^+, and OH^+ was greatly reduced [137]. Wang et al. [25] further studied the reaction pathways of CH_3OH production over Cu/Al_2O_3 catalyst and DBD plasma. In the plasma-alone system, HCO as a crucial intermediate could be formed by the combination of CO and H; however, the competitive recombination of H and HCO to produce CO and H_2 back would consume CO and lower the H_2CO formation rate [25,138]. In comparison, the catalyst–plasma hybrid system offered multiple reaction routes, such as CO hydrogenation and CO_2/formate hydrogenation [41], thus exhibiting a lower energy barrier and faster reaction kinetics. The necessity of the integration of DBD plasma and the catalysts was emphasized via one-dimensional fluid model [27]. In detail, CO was the only value-added product in plasma-alone system with a CO_2/H_2 feed due to the deficient CH_2 radicals, which was abundant in the CO_2/CH_4 mixture. Thus, a CO_2/H_2 mixed feed might not be suitable as a CO_2/CH_4 combination if other value-added chemicals were the main target, such as CH_3OH. However, the selectivity of certain oxygenates would be enhanced when the plasma was coupled with the catalyst [72].

As for the CH_4 production via CO_2 hydrogenation, one mechanism based on Ni-based catalysts was ever proposed that CO was first produced from the electron-impact dissociation of CO_2 and existed in the form of monodentate formates in gaseous state or adsorbed on the Ni surface. Under the DBD plasma, the formates were converted to linear carbonyls, which were further hydrogenated to generate CH_4 through stepwise recombination with H radicals [64]. The beneficial effect of DBD plasma was proven by Mu et al. [139] that the rate-determining step for CO_2 methanation was the dissociation of adsorbed H_2 and CO_2 on the Ni surface [63]. Assisted by the plasma, the activation energy was significantly decreased from 80 to 29 kJ/mol, thus promoting the facilitated dissociation of CO_2 and H_2 to form reactive CO and H species, which subsequently combined to produce CH_x and CH_4. Benefiting from the rapid O removal, CO_2 dissociation turned out to be irreversible, improving the reaction kinetics and selectivity [49].

7. Conclusive Remarks and Prospects

In this review, an overview is first provided regarding the plasma and catalyst-plasma hybrid system in CO_2 hydrogenation. After that, main contents were placed on the synergy between the catalyst and DBD plasma, including active metals, supports, and additives. Simultaneously, the structure–performance relationships are elucidated in depth. The plasma–catalyst hybrid system affected the reaction route and performance in a synergistic manner that the DBD plasma modified the dispersion of the active site, surface basicity, and oxygen defects; in turn, the plasma property (e.g., input power and ionization energy) could be adjusted by the ionic conductivity and dielectric constants of different catalysts, resulting in various degrees of energy utilization. Subsequently, the influences of operation parameters (e.g., applied voltage, input power, feed ratio, GHSV) and reactor configurations (membrane-assisted DBD reactor, adiabatic reactor, two-stage reactor) on the catalytic performances and energy efficiencies are discussed in detail. In addition, various mechanisms of CO_2 hydrogenation based on two targeted products of CH_4 and CH_3OH are demonstrated. Despite the improvements in plasma–catalytic CO_2 hydrogenation, some issues still exist and the possible solutions are proposed as below.

First, there is still no agreement regarding the synergy between the surface basicity of catalysts and DBD plasma. Advanced characterization techniques (e.g., CO_2-TPD, in-situ FT-IR) and numerical studies based on appropriate models are promising potential solutions.

Second, the general relationship between the input power/applied voltage and the catalytic performances are still under debate. An intensified ionization process might lead to an efficient activation and dissociation of CO_2 while the possible decomposition of the products under this condition is a concern. Depending on the specific catalytic system and targeted product, the desired operation parameters (e.g., input power) are waiting for further explorations via advanced mathematical tools.

Third, as a newly emerging catalysis, plasma catalysis requires tremendous effort to realize its commercialization, by means of enhancing the energy efficiency, exploiting efficient production of H_2 from renewable energy sources, and increasing the selectivity of value-added products based on a thorough investigation of the mechanisms.

Fourth, the origin of the plasma enhancement, at least in some systems, is an important yet unresolved question. Thus, more studies might be needed in the future.

Author Contributions: X.G.: conceptualization, data curation, investigation, writing—original draft, writing—review and editing; J.L.: conceptualization, data curation, investigation, writing—original draft, writing—review and editing; L.W. (Liqing Wu): data curation, writing—original draft; L.W. (Lixia Wu): data curation; S.K.: funding acquisition, resources, project administration, supervision, validation. All authors have read and agreed to the published version of the manuscript.

Data Availability Statement: All data included in this study are available upon request from the publishers.

Conflicts of Interest: The authors declare no conflict of interest.

References

1. Liu, M.; Yi, Y.; Wang, L.; Guo, H.; Bogaerts, A. Hydrogenation of Carbon Dioxide to Value-Added Chemicals by Heterogeneous Catalysis and Plasma Catalysis. *Catalysts* **2019**, *9*, 275. [CrossRef]
2. Anoop, N.; Sundaramurthy, S.; Jha, J.M.; Chandrabalan, S.; Singh, N.; Verma, J.; Parvatalu, D.; Katti, S. Plasma catalysis: A feasible solution for carbon dioxide valorization? *Clean Technol. Envir.* **2021**, *23*, 2789–2811. [CrossRef]
3. Irish, J.L.; Sleath, A.; Cialone, M.A.; Knutson, T.R.; Jensen, R.E. Simulations of Hurricane Katrina (2005) under sea level and climate conditions for 1900. *Clim. Chang.* **2014**, *122*, 635–649. [CrossRef]

4. Bobicki, E.R.; Liu, Q.; Xu, Z.; Zeng, H. Carbon capture and storage using alkaline industrial wastes. *Prog. Energy Combust. Sci.* **2012**, *38*, 302–320. [CrossRef]

5. Rahman, F.A.; Aziz, M.M.A.; Saidur, R.; Wan, W.A.; Hainin, M.R.; Putrajava, R.; Hassan, N.A. Pollution to solution: Capture and sequestration of carbon dioxide (CO_2) and its utilization as a renewable energy source for a sustainable future. *Renew. Sustain. Energy Rev.* **2017**, *71*, 112–126. [CrossRef]

6. Snoeckx, R.; Bogaerts, A. Plasma technology—a novel solution for CO_2 conversion? *Chem. Soc. Rev.* **2017**, *46*, 5805–5863. [CrossRef] [PubMed]

7. Chen, H.; Mu, Y.; Xu, S.; Xu, S.; Hardacre, C.; Fan, X. Recent advances in non-thermal plasma (NTP) catalysis towards C1 chemistry. *Chin. J. Chem. Eng.* **2020**, *28*, 2010–2021. [CrossRef]

8. Xu, S.; Chen, S.; Hardacre, C.; Fan, X. Non-thermal plasma catalysis for CO_2 conversion and catalyst design for the process. *J. Phys. D Appl. Phys.* **2021**, *54*, 233001. [CrossRef]

9. Ashok, J.; Ang, M.L.; Kawi, S. Enhanced activity of CO_2 methanation over Ni/ CeO_2–ZrO_2 catalysts: Influence of preparation methods. *Catal. Today* **2017**, *281*, 304–311. [CrossRef]

10. Ashok, J.; Pati, S.; Hongmanorom, P.; Zhang, T.; Chen, J.; Kawi, S. A review of recent catalyst advances in CO_2 methanation processes. *Catal. Today* **2020**, *356*, 471–489. [CrossRef]

11. Bian, Z.; Chan, Y.M.; Yu, Y.; Kawi, S. Morphology dependence of catalytic properties of Ni/CeO_2 for CO_2 methanation:a kinetic and mechanism study. *Catal. Today* **2020**, *347*, 31–38. [CrossRef]

12. Dewangan, N.; Hui, W.M.; Jayaprakash, S.; Bawah, A.-R.; Poerjoto, A.J.; Jie, T.; Ashok, J.; Hidajat, K.; Kawi, S. Recent progress on layered double hydroxide (LDH) derived metal-based catalysts for CO_2 conversion to valuable chemicals. *Catal. Today* **2020**, *356*, 490–513. [CrossRef]

13. Hongmanorom, P.; Ashok, J.; Zhang, G.; Bian, Z.; Wai, M.H.; Zeng, Y.; Xi, S.; Borgna, A.; Kawi, S. Enhanced performance and selectivity of CO_2 methanation over phyllosilicate structure derived Ni–Mg/SBA-15 catalysts. *Appl. Catal. B Environ.* **2021**, *282*, 119564. [CrossRef]

14. Pati, S.; Ashok, J.; Dewangan, N.; Chen, T.; Kawi, S. Ultra-thin (similar to 1 μm) Pd–Cu membrane reactor for coupling CO_2 hydrogenation and propane dehydrogenation applications. *J. Membr. Sci.* **2020**, *595*, 117496. [CrossRef]

15. Yu, Y.; Bian, Z.; Song, F.; Wang, J.; Zhong, Q.; Kawi, S. Influence of calcination temperature on activity and selectivity of Ni–CeO_2 and Ni–$Ce_{0.8}Zr_{0.2}O_2$ catalysts for CO_2 methanation. *Top. Catal.* **2018**, *61*, 1514–1527. [CrossRef]

16. Yu, Y.; Chan, Y.M.; Bian, Z.; Song, F.; Wang, J.; Zhong, Q.; Kawi, S. Enhanced performance and selectivity of CO_2 methanation over g-C_3N_4 assisted synthesis of Ni–CeO_2 catalyst: Kinetics and DRIFTS studies. *Int. J. Hydrog. Energy* **2018**, *43*, 15191–15204. [CrossRef]

17. Poerjoto, A.J.; Ashok, J.; Dewangan, N.; Kawi, S. The role of lattice oxygen in CO_2 hydrogenation to methanol over $La_{1−x}Sr_xCuO$ catalysts. *J. CO_2 Util.* **2021**, *47*, 101498. [CrossRef]

18. Wang, Y.; Gao, W.; Li, K.; Zheng, Y.; Xie, Z.; Na, W.; Chen, J.G.; Wang, H. Strong Evidence of the Role of H_2O in Affecting Methanol Selectivity from CO_2 Hydrogenation over Cu–ZnO–ZrO_2. *Chem* **2020**, *6*, 419–430. [CrossRef]

19. Li, Z.; Deng, Y.; Dewangan, N.; Hu, J.; Wang, Z.; Tan, X.; Liu, X.; Kawi, S. High Temperature Water Permeable Membrane Reactors for CO_2 Utilization. *Chem. Eng. J.* **2021**, *420*, 129834. [CrossRef]

20. Hongmanorom, P.; Ashok, J.; Chirawatkul, P.; Kawi, S. Interfacial synergistic catalysis over Ni nanoparticles encapsulated in mesoporous ceria for CO_2 methanation. *Appl. Catal. B Environ.* **2021**, *297*, 120454. [CrossRef]

21. Ashok, J.; Das, S.; Dewangan, N.; Hongmanorom, P.; Wai, M.H.; Kawi, S. Conversion of CO_2 to C-1 chemicals: Catalyst design, kinetics and mechanism aspects of the reactions. *Catal. Today* **2020**, *358*, 3–29.

22. Wai, M.H.; Ashok, J.; Dewangan, N.; Das, S.; Xi, S.; Borgna, A.; Kawi, S. Influence of Surface Formate Species on Methane Selectivity for Carbon Dioxide Methanation over Nickel Hydroxyapatite Catalyst. *ChemCatChem* **2020**, *12*, 6410–6419. [CrossRef]

23. Gao, X.; Li, J.; Zheng, M.; Cai, S.; Zhang, J.; Askari, S.; Dewangan, N.; Ashok, J.; Kawi, S. Recent progress in anti-coking Ni catalysts for thermo-catalytic conversion of greenhouse gases. *Process Saf. Environ.* **2021**, *156*, 598–616. [CrossRef]

24. Wang, W.; Wang, S.; Ma, X.; Gong, J. Recent advances in catalytic hydrogenation of carbon dioxide. *Chem. Soc. Rev.* **2011**, *40*, 3703–3727. [CrossRef]

25. Wang, L.; Yi, Y.; Guo, H.; Tu, X. Atmospheric pressure and room temperature synthesis of methanol through plasma–catalytic hydrogenation of CO_2. *ACS Catal.* **2018**, *8*, 90–100. [CrossRef]

26. Eliasson, B.; Kogelschatz, U.; Xue, B.; Zhou, L.-M. Hydrogenation of carbon dioxide to methanol with a discharge-activated catalyst. *Ind. Eng. Chem. Res.* **1998**, *37*, 3350–3357. [CrossRef]

27. De Bie, C.; van Dijk, J.; Bogaerts, A. CO_2 hydrogenation in a dielectric barrier discharge plasma revealed. *J. Phys. Chem. C* **2016**, *120*, 25210–25224. [CrossRef]

28. Zhao, B.; Liu, Y.; Zhu, Z.; Guo, H.; Ma, X. Highly selective conversion of CO_2 into ethanol on Cu/ZnO/Al_2O_3 catalyst with the assistance of plasma. *J. CO_2 Util.* **2018**, *24*, 34–39. [CrossRef]

29. Dębek, R.; Azzolina-Jury, F.; Travert, A.; Maug, F. A review on plasma-catalytic methanation of carbon dioxide—Looking for an efficient catalyst. *Renew. Sust. Energ. Rev.* **2019**, *116*, 109427. [CrossRef]

30. Liu, L.; Zhang, Z.; Das, S.; Kawi, S. Reforming of tar from biomass gasification in a hybrid catalysis–plasma system: A review. *Appl. Catal. B Environ.* **2019**, *250*, 250–272. [CrossRef]

31. Li, Z.; Lin, Q.; Li, M.; Cao, J.; Liu, F.; Pan, H.; Wang, Z.; Kawi, S. Recent advances in process and catalyst for CO_2 reforming of methane. *Renew. Sust. Energ. Rev.* **2020**, *134*, 110312. [CrossRef]

32. Liu, L.; Zhang, Z.; Das, S.; Xi, S.; Kawi, S. $LaNiO_3$ as a precursor of Ni/La_2O_3 for reverse water–gas shift in DBD plasma: Effect of calcination temperature. *Energy Convers. Manag.* **2020**, *206*, 112475. [CrossRef]

33. Ashok, J.; Kawi, S. Low-temperature biomass tar model reforming over perovskite materials with DBD plasma: Role of surface oxygen mobility. *Energ. Convers. Manag.* **2021**, *248*, 114802. [CrossRef]

34. Kawi, S.; Ashok, J.; Dewangan, N.; Pati, S.; Chen, J. Recent Advances in Catalyst Technology for Biomass Tar Model Reforming: Thermal, Plasma and Membrane Reactors. *Waste Biomass Valori.* **2021**. [CrossRef]

35. Liu, L.; Das, S.; Chen, T.; Dewangan, N.; Ashok, J.; Xi, S.; Borgna, A.; Li, Z.; Kawi, S. Low temperature catalytic reverse water-gas shift reaction over perovskite catalysts in DBD plasma. *Appl. Catal. B Environ.* **2020**, *265*, 118573. [CrossRef]

36. Kawi, S.; Kathiraser, Y.; Ni, J.; Oemar, U.; Li, Z.; Saw, E.T. Progress in Synthesis of Highly Active and Stable Nickel-Based Catalysts for Carbon Dioxide Reforming of Methane. *ChemSusChem* **2015**, *8*, 3556–3575. [CrossRef]

37. Lee, C.J.; Lee, D.H.; Kim, T. Enhancement of methanation of carbon dioxide using dielectric barrier discharge on a ruthenium catalyst at atmospheric conditions. *Catal. Today* **2017**, *293–294*, 97–104. [CrossRef]

38. Bogaerts, A.; Kozák, T.; van Laer, K.; Snoeckx, R. Plasma-based conversion of CO_2: Current status and future challenges. *Faraday Discuss.* **2015**, *183*, 217–232. [CrossRef]

39. Gao, X.; Lin, Z.; Li, T.; Huang, L.; Zhang, J.; Askari, S.; Dewangan, N.; Ashok, J.; Kawi, S. Recent Developments in Dielectric Barrier Discharge Plasma-Assisted Catalytic Dry Reforming of Methane over Ni-Based Catalysts. *Catalysts* **2021**, *11*, 455. [CrossRef]

40. Yuan, H.; Zhu, X.; Han, J.; Wang, H.; Ge, Q. Rhenium-promoted selective CO_2 methanation on Ni-based catalyst. *J. CO_2 Util.* **2018**, *26*, 8–18. [CrossRef]

41. Kattel, S.; Yan, B.; Chen, J.G.; Liu, P. CO_2 hydrogenation on Pt, Pt/SiO_2 and Pt/TiO_2: Importance of synergy between Pt and oxide support. *J. Catal.* **2016**, *343*, 115–126. [CrossRef]

42. Bogaerts, A.; Neyts, E.; Gijbels, R.; Van der Mullen, J. Gas discharge plasmas and their applications. *Spectrochim. Acta Part B* **2002**, *57*, 609–658. [CrossRef]

43. Chen, H.L.; Lee, H.M.; Chen, S.H.; Chang, M.B.; Yu, S.J.; Li, S.N. Removal of Volatile Organic Compounds by Single-Stage and Two-Stage Plasma Catalysis Systems: A Review of the Performance Enhancement Mechanisms, Current Status, and Suitable Applications. *Environ. Sci. Technol.* **2009**, *43*, 2216–2227. [CrossRef]

44. Patil, B.S.; Cherkasov, N.; Lang, J.; Ibhadon, A.O.; Hessel, V.; Wang, Q. Low temperature plasma–catalytic NO_x synthesis in a packed DBD reactor: Effect of support materials and supported active metal oxides. *Appl. Catal. B Environ.* **2016**, *194*, 123–133. [CrossRef]

45. Suttikul, T.; Nuchdang, S.; Rattanaphra, D.; Phalakornkule, C. Influence of Operating Parameters, Al_2O_3 and Ni/Al_2O_3 Catalysts on Plasma Assisted CO_2 Reforming of CH_4 in a Parallel Plate Dielectric Barrier Discharge for High H_2/CO Ratio Syngas Production. *Plasma Chem. Plasma Process.* **2020**, *40*, 1445–1463. [CrossRef]

46. Whitehead, J.C. Plasma–catalysis: The known knowns, the known unknowns and the unknown unknowns. *J. Phys. D Appl. Phys.* **2016**, *49*, 243001. [CrossRef]

47. Ahmad, F.; Lovell, E.C.; Masood, H.; Cullen, P.J.; Ostrikov, K.K.; Scott, J.A.; Amal, R. Low-temperature CO_2 methanation: Synergistic effects in plasma–Ni hybrid catalytic system. *ACS Sustain. Chem. Eng.* **2020**, *8*, 1888–1898. [CrossRef]

48. Neyts, E.C. Plasma–surface interactions in plasma catalysis. *Plasma Chem. Plasma Process.* **2015**, *36*, 185–212. [CrossRef]

49. Mikhail, M.; Wang, B.; Jalain, R.; Cavadias, S.; Tatoulian, M.; Ognier, S.; Gálvez, M.E.; da Costa, P. Plasma–catalytic hybrid process for CO_2 methanation: Optimization of operation parameters. *React. Kinet. Mech. Catal.* **2019**, *126*, 629–643. [CrossRef]

50. Debek, R.; Wierzbicki, D.; Motak, M.; Galvez, M.E.; Costa, P.D.; Azzolina-Jury, F. Operando FT-IR study on basicity improvement of Ni(Mg,Al)O hydrotalcite-derived catalysts promoted by glow plasma discharge. *Plasma Sci. Technol.* **2019**, *21*, 045503. [CrossRef]

51. Dębek, R.; Azzolina-Jury, F.; Travert, A.; Maugé, F.; Thibault-Starzyk, F. Low-pressure glow discharge plasma-assisted catalytic CO_2 hydrogenation – the effect of metal oxide support on the performance of the Ni-based catalyst. *Catal. Today* **2019**, *337*, 182–194. [CrossRef]

52. Parastaev, A.; Hoeben, W.F.L.M.; van Heesch, B.E.J.M.; Kosinov, N.; Hensen, E.J.M. Temperature-programmed plasma surface reaction: An approach to determine plasma–catalytic performance. *Appl. Catal. B Environ.* **2018**, *239*, 168–177. [CrossRef]

53. Men, Y.-L.; Liu, Y.; Wang, Q.; Luo, Z.-H.; Shao, S.; Li, Y.-B.; Pan, Y.-X. Highly dispersed Pt-based catalysts for selective CO_2 hydrogenation to methanol at atmospheric pressure. *Chem. Eng. Sci.* **2019**, *200*, 167–175. [CrossRef]

54. Liao, F.; Wu, X.P.; Zheng, J.; Li, M.M.J.; Kroner, A.; Zeng, Z.; Hong, X.; Yuan, Y.; Gong, X.Q.; Tsang, S.C.E. A promising low pressure methanol synthesis route from CO_2 hydrogenation over Pd@Zn core–shell catalysts. *Green Chem.* **2017**, *19*, 270–280. [CrossRef]

55. Zeng, Y.; Tu, X. Plasma–catalytic hydrogenation of CO_2 for the cogeneration of CO and CH_4 in a dielectric barrier discharge reactor: Effect of argon addition. *J. Phys. D Appl. Phys.* **2017**, *50*, 184004. [CrossRef]

56. Zhang, S.; Li, L.; Zhao, S.; Sun, Z.; Luo, J. Construction of Interpenetrated Ruthenium Metal–Organic Frameworks as Stable Photocatalysts for CO_2 Reduction. *Inorg. Chem.* **2015**, *54*, 8375–8379. [CrossRef] [PubMed]

57. Xu, W.; Zhang, X.; Dong, M.; Zhao, J.; Di, L. Plasma-assisted Ru/Zr-MOF catalyst for hydrogenation of CO_2 to methane. *Plasma Sci. Technol.* **2019**, *21*, 044004. [CrossRef]

58. Lan, L.; Wang, A.; Wang, Y. CO$_2$ hydrogenation to lower hydrocarbons over ZSM-5-supported catalysts in a dielectric-barrier discharge plasma reactor. *Catal. Commun.* **2019**, *130*, 105761. [CrossRef]

59. Wang, J.; AlQahtani, M.S.; Wang, X.; Knecht, S.D.; Bilén, S.G.; Song, C.; Chu, W. One-step plasma-enabled catalytic carbon dioxide hydrogenation to higher hydrocarbons: Significance of catalyst-bed configuration. *Green Chem.* **2021**, *23*, 1642–1647. [CrossRef]

60. Chen, H.; Mu, Y.; Shao, Y.; Chansai, S.; Xiang, H.; Jiao, Y.; Hardacre, C.; Fan, X. Nonthermal plasma (NTP) activated metal–organic frameworks (MOFs) catalyst for catalytic CO$_2$ hydrogenation. *AIChE J.* **2020**, *66*, e16853. [CrossRef]

61. Bacariza, M.C.; Biset-Peiró, M.; Graça, I.; Guilera, J.; Morante, J.; Lopes, J.M.; Andreu, T.; Henriques, C. DBD plasma-assisted CO$_2$ methanation using zeolite-based catalysts: Structure composition–reactivity approach and effect of Ce as promoter. *J. CO$_2$ Util.* **2018**, *26*, 202–211. [CrossRef]

62. Biset-Peiró, M.; Guilera, J.; Zhang, T.; Arbiol, J.; Andreu, T. On the role of ceria in Ni–Al$_2$O$_3$ catalyst for CO$_2$ plasma methanation. *Appl. Catal. A Gen.* **2019**, *575*, 223–229. [CrossRef]

63. Chen, H.; Mu, Y.; Shao, Y.; Chansai, S.; Xu, S.; Stere, C.E.; Xiang, H.; Zhang, R.; Jiao, Y.; Hardacre, C.; et al. Coupling non-thermal plasma with Ni catalysts supported on BETA zeolite for catalytic CO$_2$ methanation. *Catal. Sci. Technol.* **2019**, *9*, 4135–4145. [CrossRef]

64. Wierzbicki, D.; Moreno, M.V.; Ognier, S.; Motak, M.; Grzybek, T.; Da Costa, P.; Gálvez, M.E. Ni-Fe layered double hydroxide derived catalysts for non-plasma and DBD plasma-assisted CO$_2$ methanation. *Int. J. Hydrog. Energy* **2020**, *45*, 10423–10432. [CrossRef]

65. Mikhail, M.; Da Costa, P.; Amouroux, J.; Cavadias, S.; Tatoulian, M.; Ognier, S.; Gálvez, M.E. Effect of Na and K impurities on the performance of Ni/CeZrO$_x$ catalysts in DBD plasma–catalytic CO$_2$ methanation. *Fuel* **2021**, *306*, 121639. [CrossRef]

66. Kattel, S.; Yan, B.; Yang, Y.; Chen, J.G.; Liu, P. Optimizing Binding Energies of Key Intermediates for CO$_2$ Hydrogenation to Methanol over Oxide-Supported Copper. *J. Am. Chem. Soc.* **2016**, *138*, 12440–12450. [CrossRef] [PubMed]

67. Xiao, S.; Zhang, Y.; Gao, P.; Zhong, L.; Li, X.; Zhang, Z.; Wang, H.; Wei, W.; Sun, Y. Highly efficient Cu-based catalysts via hydrotalcite-like precursors for CO$_2$ hydrogenation to methanol. *Catal. Today* **2017**, *281*, 327–336. [CrossRef]

68. Behrens, M.; Studt, F.; Kasatkin, I.; Kühl, S.; Hävecker, M.; Abild-Pedersen, F.; Zander, S.; Girgsdies, F.; Kurr, P.; Kniep, B.-L.; et al. The Active Site of Methanol Synthesis over Cu/ZnO/Al$_2$O$_3$ Industrial Catalysts. *Science* **2012**, *336*, 893–897. [CrossRef]

69. Fichtl, M.B.; Schumann, J.; Kasatkin, I.; Jacobsen, N.; Behrens, M.; Schlögl, R.; Muhler, M.; Hinrichsen, O. Counting of Oxygen Defects versus Metal Surface Sites in Methanol Synthesis Catalysts by Different Probe Molecules. *Angew. Chem. Int. Ed.* **2014**, *53*, 7043–7047. [CrossRef]

70. Studt, F.; Sharafutdinov, I.; Abild-Pedersen, F.; Elkjar, C.F.; Hummelshoj, J.S.; Dahl, S.; Chorkendorff, I.; Norskov, J.K. Discovery of a Ni–Ga catalyst for carbon dioxide reduction to methanol. *Nat. Chem.* **2014**, *6*, 320–324. [CrossRef] [PubMed]

71. Feliz, M.Q.; Polaert, I.; Ledoux, A.; Fernandez, C.; Azzolina-Jury, F. Influence of ionic conductivity and dielectric constant of the catalyst on DBD plasma-assisted CO$_2$ hydrogenation into methanol. *J. Phys. D Appl. Phys.* **2021**, *54*, 334003. [CrossRef]

72. Zeng, Y.; Tu, X. Plasma–Catalytic CO$_2$ Hydrogenation at Low Temperatures. *IEEE T. Plasma Sci.* **2016**, *44*, 405–411. [CrossRef]

73. Liu, C.; Cundari, T.R.; Wilson, A.K. Reaction mechanism of the reverse water–gas shift reaction using first-row middle transition metal catalysts L'M (M = Fe, Mn, Co): A computational study. *Inorg. Chem.* **2011**, *50*, 8782–8789. [CrossRef] [PubMed]

74. Wang, W.; Gong, J. Methanation of carbon dioxide: An overview. *Front. Chem. Sci. Eng.* **2011**, *5*, 2–10.

75. Saeidi, S.; Aishah, N.; Amin, S.; Rahimpour, M.R. Hydrogenation of CO$_2$ to valueadded products—A review and potential future developments. *Biochem. Pharmacol.* **2014**, *5*, 66–81.

76. Vosoughi, V.; Dalai, A.K.; Abatzoglou, N.; Hu, Y. Performances of promoted cobalt catalysts supported on mesoporous alumina for Fischer–Tropsch synthesis. *Appl. Catal. A Gen.* **2017**, *547*, 155–163. [CrossRef]

77. Azzolina-Jury, F.; Bento, D.; Henriques, C.; Thibault-Starzyk, F. Chemical Engineering Aspects of Plasma-Assisted CO$_2$ hydrogenation over Nickel Zeolites under Partial Vacuum. *J. CO$_2$ Util.* **2017**, *22*, 97–109. [CrossRef]

78. Benrabbah, R.; Cavaniol, C.; Liu, H.; Ognier, S.; Cavadias, S.; Gálvez, M.E.; Da Costa, P. Plasma DBD Activated Ceria–Zirconia-Promoted Ni-Catalysts for Plasma Catalytic CO$_2$ hydrogenation at Low Temperature. *Catal. Commun.* **2017**, *89*, 73–76. [CrossRef]

79. Bal, K.M.; Huygh, S.; Bogaerts, A.; Neyts, E.C. Effect of Plasma-Induced Surface Charging on Catalytic Processes: Application to CO$_2$ activation. *Plasma Sources mnopSci. Technol.* **2018**, *27*, 024001. [CrossRef]

80. Kim, J.; Abbott, M.S.; Go, D.B.; Hicks, J.C. Enhancing C−H Bond Activation of Methane via Temperature-Controlled, Catalyst−Plasma Interactions. *ACS Energy Lett.* **2016**, *1*, 94–99. [CrossRef]

81. Jiang, N.; Qiu, C.; Guo, L.; Shang, K.; Lu, N.; Li, J.; Zhang, Y.; Wu, Y. Plasma-Catalytic Destruction of Xylene over Ag–Mn Mixed Oxides in a Pulsed Sliding Discharge Reactor. *J. Hazard. Mater.* **2019**, *369*, 611–620. [CrossRef]

82. Mehta, P.; Barboun, P.; Go, D.B.; Hicks, J.C.; Schneider, W.F. Catalysis Enabled by Plasma Activation of Strong Chemical Bonds: A Review. *ACS Energy Lett.* **2019**, *4*, 1115–1133. [CrossRef]

83. Wang, X.; Shi, H.; Szanyi, J. Controlling Selectivities in CO$_2$ Reduction through Mechanistic Understanding. *Nat. Commun.* **2017**, *8*, 1–6. [CrossRef] [PubMed]

84. Shirazi, M.; Bogaerts, A.; Neyts, E.C. A DFT Study of H-Dissolution into the Bulk of a Crystalline Ni(111) Surface: A Chemical Identifier for the Reaction Kinetics. *Phys. Chem. Chem. Phys.* **2017**, *19*, 19150–19158. [CrossRef]

85. Shirazi, M.; Neyts, E.C.; Bogaerts, A. DFT Study of Ni-Catalyzed Plasma Dry Reforming of Methane. *Appl. Catal. B Environ.* **2017**, *205*, 605–614. [CrossRef]

86. Butterworth, T.; Elder, R.; Allen, R. Effects of Particle Size on CO_2 reduction and Discharge Characteristics in a Packed Bed Plasma Reactor. *Chem. Eng. J.* **2016**, *293*, 55–67. [CrossRef]

87. Zhang, Y.R.; Neyts, E.C.; Bogaerts, A. Influence of the Material Dielectric Constant on Plasma Generation inside Catalyst Pores. *J. Phys. Chem. C* **2016**, *120*, 25923–25934. [CrossRef]

88. Jwa, E.; Lee, S.B.; Lee, H.W.; Mok, Y.S. Plasma-assisted catalytic methanation of CO and CO_2 over Ni–zeolite catalysts. *Fuel Process. Technol.* **2013**, *108*, 89–93. [CrossRef]

89. Chen, H.; Goodarzi, F.; Mu, Y.; Chansai, S.; Mielby, J.J.; Mao, B.; Sooknoi, T.; Hardacre, C.; Kegnæs, S.; Fan, X. Effect of metal dispersion and support structure of Ni/silicalite-1 catalysts on non-thermal plasma (NTP) activated CO_2 hydrogenation. *Appl. Catal. B Environ.* **2020**, *272*, 119013. [CrossRef]

90. Whitehead, J.C. Plasma–catalysis: Is it just a question of scale? *Front. Chem. Sci. Eng.* **2019**, *13*, 264–273. [CrossRef]

91. Christensen, P.A.; Ali, A.H.B.M.; Mashhadani, Z.T.A.W.; Carroll, M.A.; Martin, P.A. The Production of Ketene and C_5O_2 from CO_2, N_2 and CH_4 in a Non-thermal Plasma Catalysed by Earth-Abundant Elements: An In-Situ FTIR Study. *Plasma Chem. Plasma Process.* **2018**, *38*, 461–484. [CrossRef]

92. Yan, X.; Liu, Y.; Zhao, B.; Wang, Z.; Wang, Y.; Liu, C.-J. Methanation over Ni/SiO_2: Effect of the catalyst preparation methodologies. *Int. J. Hydrog. Energy* **2013**, *38*, 2283–2291. [CrossRef]

93. Fan, Z.; Sun, K.; Rui, N.; Zhao, B.; Liu, C.-J. Improved activity of $Ni/MgAl_2O_4$ for CO_2 methanation by the plasma decomposition. *J. Energy Chem.* **2015**, *24*, 655–659. [CrossRef]

94. Neyts, E.C.; Bogaerts, A. Understanding plasma catalysis through modelling and simulation—A review. *J. Phys. D Appl. Phys.* **2014**, *47*, 224010. [CrossRef]

95. Butterworth, T.; Allen, R.W.K. Plasma–catalyst interaction studied in a single pellet DBD reactor: Dielectric constant effect on plasma dynamics. *Plasma Sources Sci. Technol.* **2017**, *26*, 065008. [CrossRef]

96. Mei, D.; Zhu, X.; He, Y.-L.; Yan, J.D.; Tu, X. Plasma-assisted conversion of CO_2 in a dielectric barrier discharge reactor: Understanding the effect of packing materials. *Plasma Sources Sci. Technol.* **2014**, *24*, 015011. [CrossRef]

97. Wang, W.; Kim, H.-H.; van Laer, K.; Bogaerts, A. Streamer propagation in a packed bed plasma reactor for plasma catalysis applications. *Chem. Eng. J.* **2018**, *334*, 2467–2479. [CrossRef]

98. Nilsson, M.; Jozsa, P.; Pettersson, L.J. Evaluation of Pd-based catalysts and the influence of operating conditions for autothermal reforming of dimethyl ether. *Appl. Catal. B Environ.* **2007**, *76*, 42–50. [CrossRef]

99. Kuld, S.; Thorhauge, M.; Falsig, H.; Elkjær, C.F.; Helveg, S.; Chorkendorff, I.; Sehested, J. Quantifying the promotion of Cu catalysts by ZnO for methanol synthesis. *Science* **2016**, *352*, 969–974. [CrossRef] [PubMed]

100. Li, J.; Sun, Y.; Wang, B.; Xiao, H.; Wu, J.; Chen, L.; Fu, M.; Ye, D. Effect of plasma on catalytic conversion of CO_2 with hydrogen over Pd/ZnO in a dielectric barrier discharge reactor. *J. Phys. D Appl. Phys.* **2019**, *52*, 244001. [CrossRef]

101. Jo, S.; Kim, T.; Lee, D.H.; Kang, W.S.; Song, Y.-H. Effect of the electric conductivity of a catalyst on methane activation in a dielectric barrier discharge reactor. *Plasma Chem. Plasma Process.* **2014**, *34*, 175–186. [CrossRef]

102. Nizio, M.; Albarazi, A.; Cavadias, S.; Amouroux, J.; Galvez, M.E.; Da Costa, P. Hybrid plasma–catalytic methanation of CO_2 at low temperature over ceria zirconia supported Ni catalysts. *Int. J. Hydrog. Energy* **2016**, *41*, 11584–11592. [CrossRef]

103. Pan, Q.; Peng, J.; Wang, S.; Wang, S. In situ FTIR spectroscopic study of the CO_2 methanation mechanism on $Ni/Ce_{0.5}Zr_{0.5}O_2$. *Catal. Sci. Technol.* **2014**, *4*, 502–509. [CrossRef]

104. Aldana, P.A.U.; Ocampo, F.; Kobl, K.; Louis, B.; Thibault-Starzyk, F.; Daturi, M.; Bazin, P.; Thomas, S.; Roger, A.C. Catalytic CO_2 valorization into CH_4 on Ni-based ceria–zirconia. Reaction mechanism by operando IR spectroscopy. *Catal. Today* **2013**, *215*, 201–207. [CrossRef]

105. Nizio, M.; Benrabbah, R.; Krzak, M.; Debek, R.; Motak, M.; Cavadias, S.; Gálvez, M.E.; Da Costa, P. Low temperature hybrid plasma–catalytic methanation over Ni–Ce–Zr hydrotalcite-derived catalysts. *Catal. Commun.* **2016**, *83*, 14–17. [CrossRef]

106. Yang, Q.; Zhang, H.-Y.; Wang, L.; Zhang, Y.; Zhao, J. Ru/UiO-66 catalyst for the reduction of nitroarenes and tandem reaction of alcohol oxidation/Knoevenagel condensation. *ACS Omega* **2018**, *3*, 4199–4212. [CrossRef] [PubMed]

107. Cavka, J.H.; Jakobsen, S.; Olsbye, U.; Guillou, N.; Lamberti, C.; Bordiga, S.; Lillerud, K.P. A new zirconium inorganic building brick forming metal organic frameworks with exceptional stability. *J. Am. Chem. Soc.* **2008**, *130*, 13850–13851. [CrossRef] [PubMed]

108. Hester, P.; Xu, S.; Liang, W.; Al-Janabi, N.; Vakili, R.; Hill, P.; Muryn, C.A.; Chen, X.; Martin, P.A.; Fan, X. On thermal stability and catalytic reactivity of Zr-based metal–organic framework (UiO-67) encapsulated Pt catalysts. *J. Catal.* **2016**, *340*, 85–94. [CrossRef]

109. Corma, A.; García, H.; Llabrés i Xamena, F.X. Engineering metal organic frameworks for heterogeneous catalysis. *Chem. Rev.* **2010**, *110*, 4606–4655. [CrossRef]

110. Xu, S.; Chansai, S.; Stere, C.; Inceesungvorn, B.; Goguet, A.; Wangkawong, K.; Rebecca Taylor, S.F.; Al-Janabi, N.; Hardacre, C.; Martin, P.A.; et al. Sustaining metal–organic frameworks for water–gas shift catalysis by non-thermal plasma. *Nat. Catal.* **2019**, *2*, 142–148. [CrossRef]

111. Rani, P.; Srivastava, R. Tailoring the catalytic activity of metal organic frameworks by tuning the metal center and basic functional sites. *New J. Chem.* **2017**, *41*, 8166–8177. [CrossRef]

112. Teeparthi, S.R.; Awin, E.W.; Kumar, R. Dominating role of crystal structure over defect chemistry in black and white zirconia on visible light photocatalytic activity. *Sci. Rep.* **2018**, *8*, 5541. [CrossRef] [PubMed]

113. Zhao, A.; Ying, W.; Zhang, H.; Ma, H.; Fang, D. $Ni–Al_2O_3$ catalysts prepared by solution combustion method for syngas methanation. *Catal. Commun.* **2012**, *17*, 34–38. [CrossRef]

114. Tada, S.; Shimizu, T.; Kameyama, H.; Haneda, T.; Kikuchi, R. Ni/CeO$_2$ catalysts with high CO$_2$ methanation activity and high CH$_4$ selectivity at low temperatures. *Int. J. Hydrog. Energy* **2011**, *37*, 5527–5531. [CrossRef]

115. Pan, Q.; Peng, J.; Sun, T.; Wang, S.; Wang, S. Insight into the reaction route of CO$_2$ methanation: Promotion effect of medium basic sites. *Catal. Commun.* **2014**, *45*, 74–78. [CrossRef]

116. Azzolina-Jury, F.; Thibault-Starzyk, F. Mechanism of Low Pressure Plasma-Assisted CO$_2$ Hydrogenation Over Ni-USY by Microsecond Time-resolved FTIR Spectroscopy. *Top. Catal.* **2017**, *60*, 1709–1721. [CrossRef]

117. Rahmani, F.; Haghighi, M.; Estifaee, P. Synthesis and characterization of Pt/Al$_2$O$_3$–CeO$_2$ nanocatalyst used for toluene abatement from waste gas streams at low temperature: Conventional vs. plasma–ultrasound hybrid synthesis methods. *Microporous Mesoporous Mater.* **2014**, *185*, 213–223. [CrossRef]

118. Liu, X.; Wang, M.; Zhou, C.; Zhou, W.; Cheng, K.; Kang, J.; Zhang, Q.; Deng, W.; Wang, Y. Selective transformation of carbon dioxide into lower olefins with a bifunctional catalyst composed of ZnGa$_2$O$_4$ and SAPO-34. *Chem. Commun.* **2017**, *54*, 140–143. [CrossRef] [PubMed]

119. Shinde, V.M.; Madras, G. Nanostructured Pd modified Ni/CeO$_2$ catalyst for water gas shift and catalytic hydrogen combustion reaction. *Appl. Catal. B Environ.* **2013**, *132–133*, 28–38. [CrossRef]

120. Bian, L.; Zhang, L.; Xia, R.; Li, Z. Enhanced low-temperature CO$_2$ methanation activity on plasma-prepared Ni-based catalyst. *J. Nat. Gas. Sci. Eng.* **2015**, *27*, 1189–1194. [CrossRef]

121. Ray, D.; Chawdhury, P.; Bhargavi, K.V.S.S.; Thatikonda, S.; Lingaiah, N.; Subrahmanyam, C. Ni and Cu oxide supported γ-Al$_2$O$_3$ packed DBD plasma reactor for CO$_2$ activation. *J. CO$_2$ Util.* **2021**, *44*, 101400. [CrossRef]

122. Schild, C.; Wokaun, A.; Baiker, A. Surface species in CO$_2$ methanation over amorphous palladium/zirconia catalysts. *J. Mol. Catal.* **1991**, *69*, 347–357. [CrossRef]

123. Wang, X.; Shi, H.; Kwak, J.H.; Szanyi, J. Mechanism of CO$_2$ Hydrogenation on Pd/Al$_2$O$_3$ Catalysts: Kinetics and Transient DRIFTS–MS Studies. *ACS Catal.* **2015**, *5*, 6337–6349. [CrossRef]

124. Mikhail, M.; Da Costa, P.; Amouroux, J.; Cavadias, S.; Tatoulian, M.; Ognier, S.; Gálvez, M.E. Electrocatalytic behaviour of CeZrO$_x$-supported Ni catalysts in plasma assisted CO$_2$ methanation. *Catal. Sci. Technol.* **2020**, *10*, 4532–4543. [CrossRef]

125. Ramakers, M.; Michielsen, I.; Aerts, R.; Meynen, V.; Bogaerts, A. Effect of Argon or Helium on the CO$_2$ Conversion in a Dielectric Barrier Discharge. *Plasma Process. Polym.* **2015**, *12*, 755–763. [CrossRef]

126. Zhang, Y.-P.; Ma, P.-S.; Zhu, X.; Liu, C.-J.; Shen, Y. A novel plasma-treated Pt/NaZSM-5 catalyst for NO reduction by methane. *Catal. Commun.* **2004**, *5*, 35–39. [CrossRef]

127. Amouroux, J.; Cavadias, S. Electrocatalytic reduction of carbon dioxide under plasma DBD process. *J. Phys. D Appl. Phys.* **2017**, *50*, 465501. [CrossRef]

128. Brooks, K.P.; Hu, J.; Zhu, H.; Kee, R.J. Methanation of carbon dioxide by hydrogen reduction using the Sabatier process in microchannel reactors. *Chem. Eng. Sci.* **2007**, *62*, 1161–1170. [CrossRef]

129. Ocampo, F.; Louis, B.; Roger, A.-C. Methanation of carbon dioxide over nickel-based Ce$_{0.72}$Zr$_{0.28}$O$_2$ mixed oxide catalysts prepared by sol–gel method. *Appl. Catal. A Gen.* **2009**, *369*, 90–96. [CrossRef]

130. Jiang, T.; Li, Y.; Liu, C.-J.; Xu, G.-H.; Eliasson, B.; Xue, B. Plasma methane conversion using dielectric-barrier discharges with zeolite A. *Catal. Today* **2002**, *72*, 229–235. [CrossRef]

131. Abate, S.; Mebrahtu, C.; Giglio, E.; Deorsola, F.; Bensaid, S.; Perathoner, S.; Pirone, R.N.; Centi, G. Catalytic Performance of γ-Al$_2$O$_3$–ZrO$_2$–TiO$_2$–CeO$_2$ Composite Oxide Supported Ni-Based Catalysts for CO$_2$ Methanation. *Ind. Eng. Chem. Res.* **2016**, *55*, 4451–4460. [CrossRef]

132. Chung, W.-C.; Chang, M.-B. Dry reforming of methane by combined spark discharge with a ferroelectric. *Energy Convers. Manag.* **2016**, *124*, 305–314. [CrossRef]

133. Biset-Peiró, M.; Mey, R.; Guilera, J.; Andreu, T. Adiabatic plasma-catalytic reactor configuration: Energy efficiency enhancement by plasma and thermal synergies on CO$_2$ methanation. *Chem. Eng. J.* **2020**, *393*, 124786. [CrossRef]

134. Chen, H.; Mu, Y.; Hardacre, C.; Fan, X. Integration of Membrane Separation with Nonthermal Plasma Catalysis: A Proof-of-Concept for CO$_2$ Capture and Utilization. *Ind. Eng. Chem. Res.* **2020**, *59*, 8202–8211. [CrossRef]

135. Poshusta, J.C.; Tuan, V.A.; Falconer, J.L.; Noble, R.D. Synthesis and permeation properties of SAPO-34 tubular membranes. *Ind. Eng. Chem. Res.* **1998**, *37*, 3924–3929. [CrossRef]

136. Li, S.; Falconer, J.L.; Noble, R.D. SAPO-34 membranes for CO$_2$/CH$_4$ separation. *J. Membr. Sci.* **2004**, *241*, 121–135. [CrossRef]

137. Liao, Y.; Zhong, W.; Qian, M.; Liu, S.; Zhang, J.; Wang, D. Numerical study on the reaction mechanism of CO$_2$ hydrogenation in atmospheric-pressure dielectric barrier discharge. *J. Appl. Phys.* **2020**, *128*, 233303. [CrossRef]

138. Gordon, E.; Ivanov, B.; Perminov, A.; Balalaev, V. A measurement of formation rates and lifetimes of intermediate complexes in reversible chemical reactions involving hydrogen atoms. *Chem. Phys.* **1978**, *35*, 79–89. [CrossRef]

139. Mu, Y.; Xu, S.; Shao, Y.; Chen, H.; Hardacre, C.; Fan, X. Kinetic Study of Nonthermal Plasma Activated Catalytic CO$_2$ Hydrogenation over Ni Supported on Silica Catalyst. *Ind. Eng. Chem. Res.* **2020**, *59*, 9478–9487. [CrossRef]